Cyclodextrin/adamantane-mediated targeting of inoculated bacteria in mice

Welling, M.M.; Duszenko, N.; Willigen, D.M. van; Smits, W.K.; Buckle, T.; Roestenberg, M.; Leeuwen, F.W.B. van

Article

Cyclodextrin/Adamantane-Mediated Targeting of Inoculated Bacteria in Mice

Mick M. Welling, Nikolas Duszenko, Danny M. van Willigen, Wiep Klaas Smits, Tessa Buckle, Meta Roestenberg, and Fijs W. B. van Leeuwen*

Read Online

ACCESS | Metrics & More | Article Recommendations | Supporting Information

ABSTRACT: Cyclodextrin (CD)-based host−guest interactions with adamantane (Ad) have demonstrated use for functionalizing living cells *in vitro*. The next step in this supramolecular functionalization approach is to explore the concept to deliver chemical cargo to living cells *in vivo*, e.g., inoculated bacteria, in order to study their dissemination. We validated this concept in two rodent *Staphylococcus aureus* models. Bacteria (1×10^8 viable *S. aureus*) were inoculated by (1) intramuscular injection or (2) intrasplenic injection followed by dissemination throughout the liver. The bacteria were prefunctionalized with ^{99m}Tc-UBI$_{29−41}$-Ad$_2$ (primary vector), which allowed us to both determine the bacterial load and create an *in vivo* target for the secondary host-vector (24 h post-inoculation). The secondary vector, i.e., chemical cargo delivery system, made use of a ^{111}In-Cy5$_{0.5}$CD$_9$PIBMA$_{39}$ polymer that was administered intravenously. Bacteria-specific cargo delivery as a result of vector complexation was evaluated by dual-isotope SPECT imaging and biodistribution studies (^{111}In), and by fluorescence (Cy5); these evaluations were performed 4 h post-injection of the secondary vector. Mice inoculated with nonfunctionalized *S. aureus* and mice without an infection served as controls. Dual-isotope SPECT imaging demonstrated that ^{111}In-Cy5$_{0.5}$CD$_9$PIBMA$_{39}$ colocalized with ^{99m}Tc-UBI$_{29−41}$-Ad$_2$-labeled bacteria in both muscle and liver. In inoculated muscle, a 2-fold higher uptake level ($3.2 \pm 1.0\%ID/g$) was noted compared to inoculation with nonfunctionalized bacteria ($1.9 \pm 0.4\%ID/g$), and a 16-fold higher uptake level compared to noninfected muscle ($0.2 \pm 0.1\%ID/g$). The hepatic accumulation of the host-vector was nearly 10-fold higher ($27.1 \pm 11.1\%ID/g$) compared to the noninfected control ($2.7 \pm 0.3\%ID/g$; $p < 0.05$). Fluorescence imaging of the secondary vector corroborated SPECT-imaging and biodistribution findings. We have demonstrated that supramolecular host−guest complexation can be harnessed to achieve an *in vivo* cargo delivery strategy, using two different bacterial models in soft tissue and liver. This proof-of-principle study paves a path toward developing innovative drug delivery concepts via cell functionalization techniques.
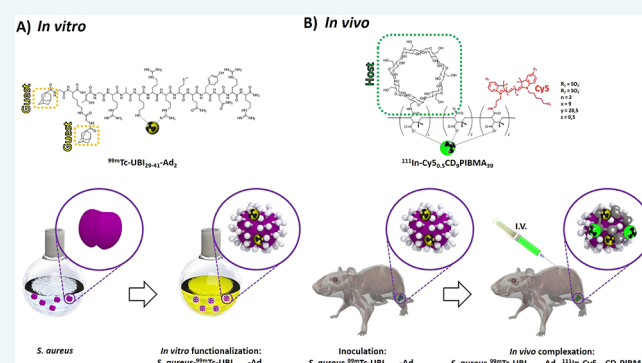
INTRODUCTION

Cyclodextrin (CD)-based host−guest supramolecular interactions with adamantane (Ad) have recently received considerable attention for the potential they hold for advancing precision medicine.[1,2] In the past, CDs' ability to bind lipophilic drugs has led to CD mostly being used to improve solubility and biodistribution.[3] More recently, CD-based host−guest chemistry has been used to create a variety of nanoparticle and surface functionalizations.[4,5] Unique to such systems is the specificity of well-defined (multivalent) host−guest interaction, which allows a wide range of functionalities, like nanoparticles or polymers, to be introduced on various surfaces.[6−8] This chemical concept has even been used to bind bacteria to functionalized surfaces.[9]

A further step has been taken by applying CD-based host−guest chemistry *in vitro* on surfaces of macroaggregated albumin microspheres (MAA; diameter 10−90 μm).[10−12]

Hepatic transplantation of Ad-functionalized MAA microspheres helped drive local accumulation of a β-CD- and Cy5-functionalized poly(isobutylene-*alt*-maleic-anhydride, PIBMA) polymer, in essence, targeted chemical cargo delivery. The PIBMA backbone of the secondary vector, first of all, serves as a backbone that connects multiple CD-host molecules, a feature that helps improve the affinity for the Ad-guest functionalized surfaces by exploiting multivalent interactions.[6] This same backbone can also serve as a carrier for various cargo molecules, e.g., fluorescent dyes and radioisotopes for
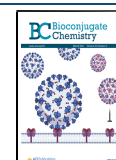
Scheme 1. Experimental Setup[a]
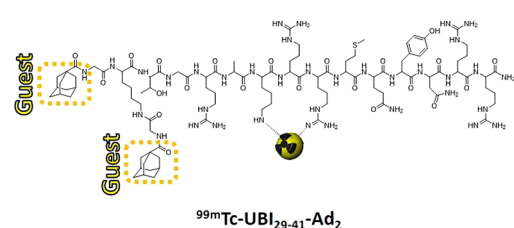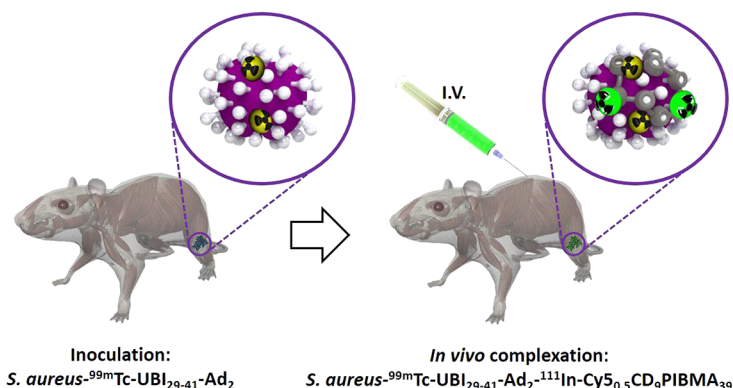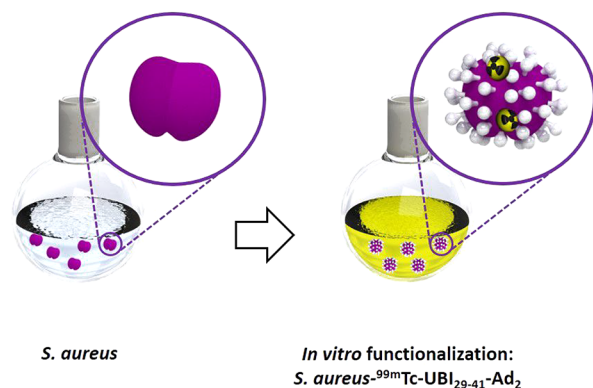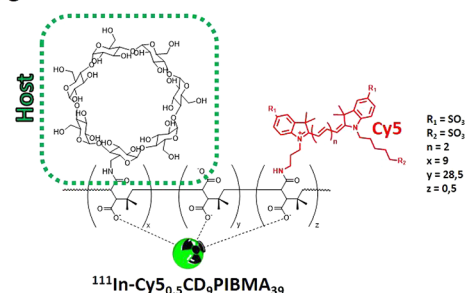
[a](A) *S. aureus* bacteria were Ad-functionalized using a ^{99m}Tc-UBI$_{29-41}$Ad$_2$ vector (guest) *in vitro*. (B) Ad-functionalized bacteria were inoculated into either thigh muscle (shown) or liver (not shown), followed by intravenous injection of a ^{111m}In-Cy5$_{0.5}$CD$_9$PIBMA$_{39}$ cargo (host). *In vivo* complexation of this host cargo with Ad-functionalized bacteria could then be assess by dual-isotope SPECT imaging.
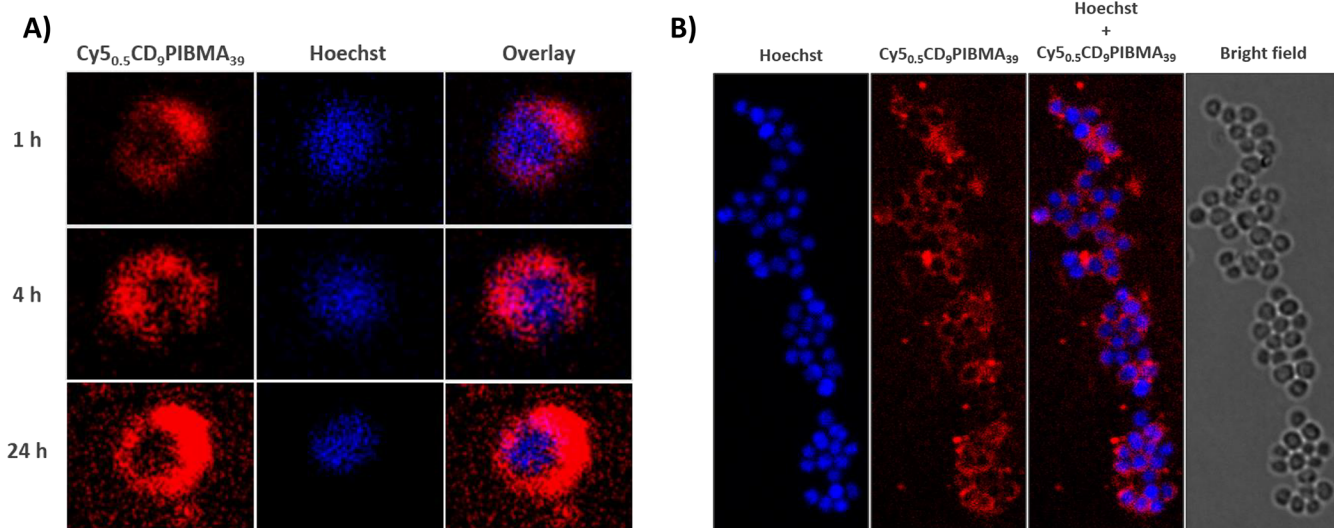

Figure 1. *In vitro* host–guest complexation in *S. aureus*. (A) Time-dependent analysis of the presence of Cy5$_{0.5}$CD$_9$PIBMA$_{39}$ complexed onto UBI$_{29-41}$-Ad$_2$-functionalized *S. aureus* over 24 h of observation. (B) Consistent complexation of host-vector Cy5$_{0.5}$CD$_9$PIBMA$_{39}$ onto UBI$_{29-41}$-Ad$_2$-functionalized bacteria after 1 h of labeling.

imaging purposes. The same host–guest chemistry has also proven to be effectively introduced *in vitro* onto the surface of mammalian cancer cells (20−30 μm diameter), macrophages (21 μm diameter), and cardiac stem cells (4−6 μm in diameter).[6,13,14] For all these cell types, host–guest chemistry created a chemical means of influencing the interaction between living cells and their environment—converting living cells into pseudochemical scaffolds suitable for supramolecular chemistry in a biological environment. Based on the above, the

next step in further developing the technology would be validating whether these pseudochemical scaffolds could be applied to deliver chemical cargos *in vivo*. Such *in vivo* cargo delivery concepts create new opportunities for more efficient delivery of, e.g., vaccines and immunomodulatory drugs, a concept we have already explored in earlier *in vitro* work in the area of host–guest functionalizations.[14]

As an extension of our earlier *in vitro* work on host–guest functionalization, we hypothesized that we could translate the
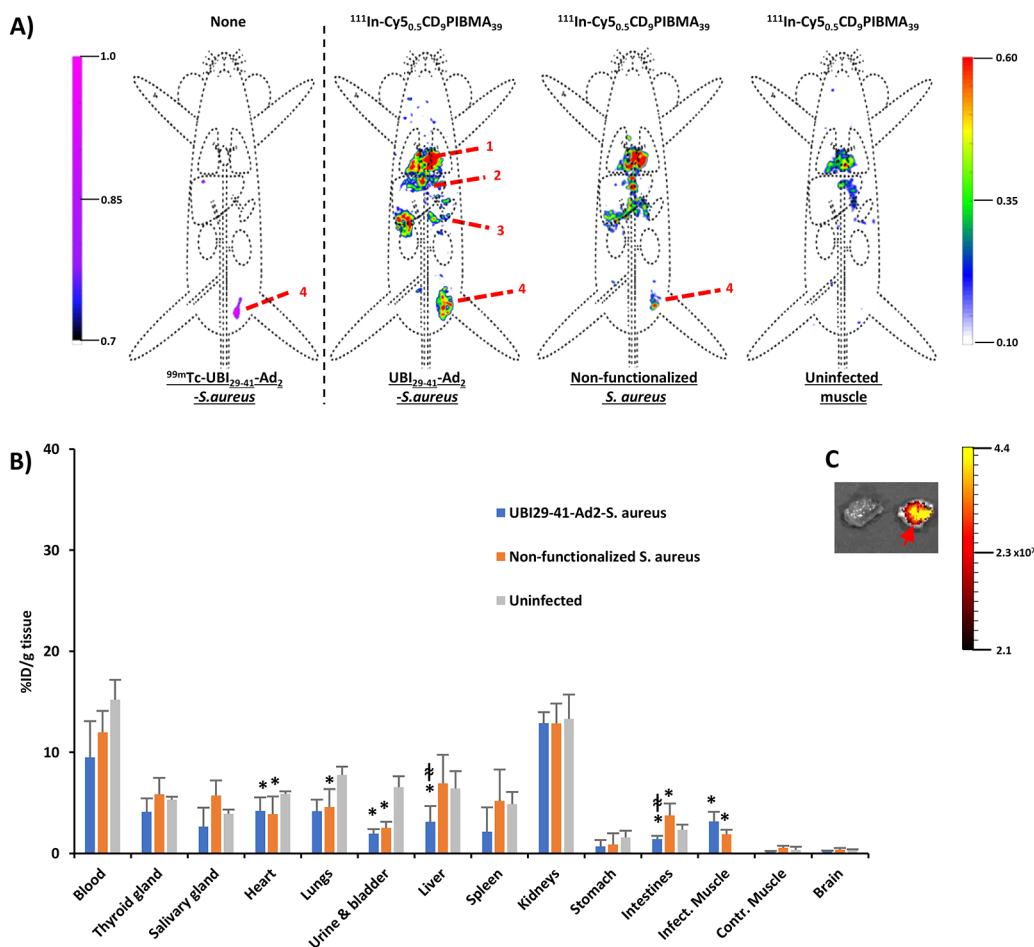
Figure 2. Cargo accumulation in bacteria-inoculated muscle. (A) *In vivo* SPECT imaging of ^{99m}Tc-UBI$_{29-41}$-Ad$_2$-labeled *S. aureus* 44 h after inoculation in the thigh muscle (left panel; purple-to-pink color coding) and imaging of host-vector ^{111}In-Cy5$_{0.5}$CD$_9$PIBMA$_{39}$ (rainbow color coding). Clear colocalization of ^{99m}Tc and ^{111}In was seen for mice colonized with Ad-functionalized *S. aureus*, whereas colocalization of such signals was less or altogether absent in nonfunctionalized bacteria or uninfected muscle, respectively. Organs are marked as (1) heart/lungs, (2) liver, (3) intestines, and (4) inoculation site (thigh muscle). (B) Biodistribution studies of ^{111}In-Cy5$_{0.5}$CD$_9$PIBMA$_{39}$ in mice inoculated with ^{99m}Tc-UBI$_{29-41}$-Ad$_2$-functionalized *S. aureus* (blue bars), nonfunctionalized *S. aureus* (orange bars), or no infection (gray bars). The data (expressed as the mean $\pm$ SD ratios of the %ID/g) showed comparable activity in blood and major tissues for the 3 groups, whereas uptake between infected muscle and controls differed significantly ($n = 6$ for each group). * $p < 0.05$. (C) *Ex vivo* fluorescence imaging of muscle tissue corroborated the these findings, with the infected muscle indicated with a red arrow. The scale bar indicates the intensity of fluorescence expressed as photons/s/cm^2.

same concept into an *in vivo* cargo delivery system. To demonstrate the proof-of-principle, we made use of *S. aureus* inoculation models where functionalized bacteria would serve as a target for the delivery of cargo. For this purpose, *S. aureus* bacteria functionalized with Ad (using the bacteria-specific UBI$_{29-41}$ vector as previously described[15]) were inoculated into thigh muscle or liver to establish infection (Scheme 1). Subsequently, this infection site, characterized by the presence of the Ad-functionalizations (the guest), then drove the local accumulation of an intravenously administered cargo, ^{111}In-Cy5$_{0.5}$CD$_9$PIBMA$_{39}$ (the host).

■ RESULTS

***In Vitro* Host−Guest Interactions.** In line with the wealth of literature that describes bacteria-specific labeling of bacterial with UBI$_{29-41}$,[16,17] *in vitro* scintillation studies revealed that the guest-vector ^{99m}Tc-UBI$_{29-41}$-Ad$_2$ gave a labeling efficiency with *S. aureus* of 86.6 $\pm$ 7.0% after 1 h of incubation, and showed that the tracer remained stably associated for at least 24 h at 37 °C (Figure S4B). Confocal microscopy confirmed binding of the host-vector (cargo) Cy5$_{0.5}$CD$_9$PIBMA$_{39}$ to UBI$_{29-41}$-Ad$_2$-

labeled *S. aureus in vitro*, with the distribution of fluorescent signals throughout the bacteria (Figure 1B); additionally, the bacterial functionalization was also shown here to remain stable for at least 24 h (Figure 1A). Localization of the host-vector Cy5$_{0.5}$CD$_9$PIBMA$_{39}$ was overwhelmingly on the bacterial surface, as evinced by the absence of overlap between Cy5 and Hoechst emissions (Figure 1A).

***In Vivo* Host−Guest Interactions.** To establish whether host−guest interactions allow for chemical cargo delivery, we subjected animal models inoculated with ^{99m}Tc-UBI$_{29-41}$-Ad$_2$-functionalized *S. aureus* (the guest) to an i.v. injection of ^{111}In-Cy5$_{0.5}$CD$_9$PIBMA$_{39}$ (the host) (Scheme 1). In the muscle inoculation model, SPECT ^{99m}Tc imaging at 24 h post-injection confirmed focal radioactivity of the ^{99m}Tc-UBI$_{29-41}$-Ad$_2$-functionalized *S. aureus* guest in the leg, though of relatively weak signal intensity after 4 physical half-lives of ^{99m}Tc (Figure 2A; left panel). At this same location, a distinct accumulation of the host ^{111}In-Cy5$_{0.5}$CD$_9$PIBMA$_{39}$ could be observed (Figure 2A). Calculations based on %ID/g data (Figure 2B, Table S1) showed that host accumulation in infected muscle was 16-fold ($p < 0.005$) higher compared to
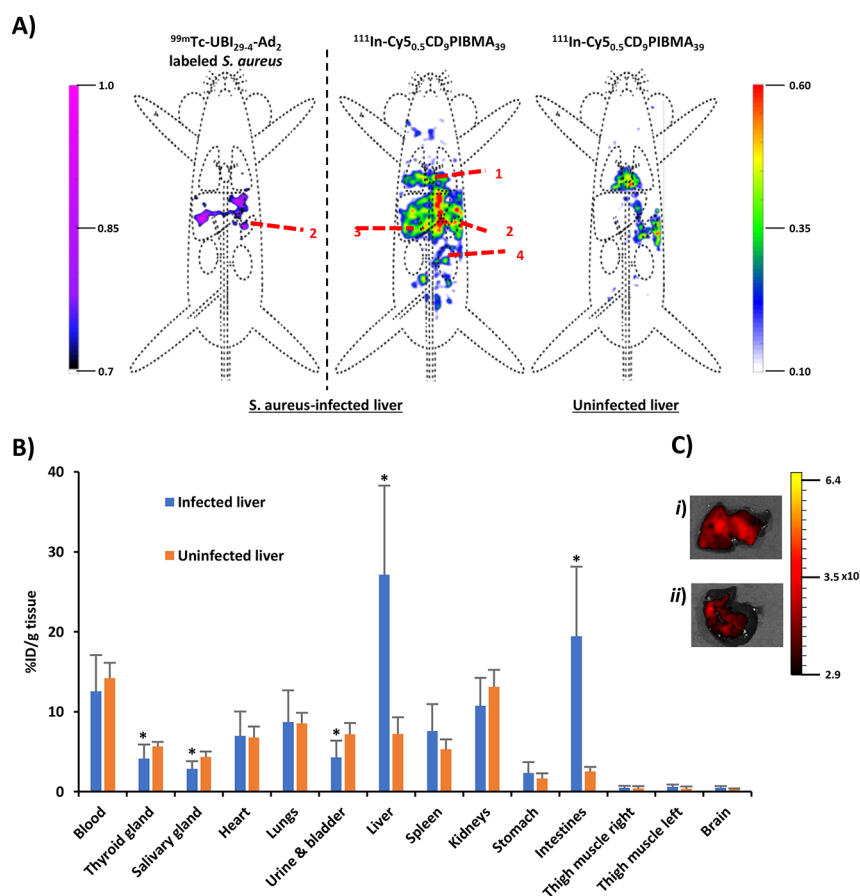
Figure 3. Cargo accumulation in the bacteria-inoculated liver. (A) SPECT imaging of ^{99m}Tc-UBI$_{29-41}$-Ad$_2$-functionalized *S. aureus* showed activity in the liver and spleen (left panel; purple-to-pink color coding). Imaging of ^{111}In-Cy5$_{0.5}$CD$_9$PIBMA$_{39}$ (rainbow color coding) showed clear colocalization in the liver (middle panel), whereas mice without infection did not show any liver colocalization (right panel). Organs are marked as (1) heart/lungs, (2) inoculation site (spleen), (3) liver, and (4) intestines. (B) Biodistribution studies of ^{111}In-Cy5$_{0.5}$CD$_9$PIBMA$_{39}$ showed significantly higher uptake in the infected liver and intestines (blue bars) compared to mice with a noninfected liver (orange bars). Data are expressed as the mean ± SD ratios of the %ID/g in the liver and blood measured at 4 h p.i. of the host-vector ($n = 6$ for each group). * $p < 0.05$. (C) *Ex vivo* fluorescence imaging of ^{111}In-Cy5$_{0.5}$CD$_9$PIBMA$_{39}$ in infected (top panel - i) and noninfected liver (bottom panel - ii). The scale bar indicates the intensity of fluorescence expressed as photons/s/cm^2.

that in contralateral uninfected muscle (3.2 ± 1.0%ID/g vs 0.2 ± 0.2%ID/g). Accumulation of ^{111}In-Cy5$_{0.5}$CD$_9$PIBMA$_{39}$ in thigh muscles of mice without an infection yielded similar uptake as the contralateral muscle, namely, 0.4 ± 0.3%ID/g. Accumulation of ^{111}In-Cy5$_{0.5}$CD$_9$PIBMA$_{39}$ in infections with UBI$_{29-41}$-Ad$_2$-functionalized *S. aureus* was 2-fold higher compared to infections with nonfunctionalized *S. aureus* (3.2 ± 1.0%ID/g vs 1.9 ± 0.4%ID/g; $p < 0.05$; 2-fold), indicating that the contribution of the functionalization step is essential in host−guest complexation *in vivo*. Fluorescence imaging confirmed these findings, with a strong Cy5 signal (host-vector) in UBI$_{29-41}$-Ad$_2$-functionalized *S. aureus*-infected muscle compared to noninfected contralateral thigh muscle (Figure 2C).

In the hepatic inoculation model, SPECT imaging (Figure 3A; left panel) of ^{99m}Tc-UBI$_{29-41}$-Ad$_2$-functionalized *S. aureus* (guest) identified radioactivity at various sites in the liver. This observation is in line with previous reports using ^{99m}Tc-Ad-MAA.[11,15] Unfortunately, the short half-life of ^{99m}Tc meant that the signal intensity in the 140 keV detection window after about 4 physical half-lives was weak (see Figure 3A). Imaging in the 240 keV window of ^{111}In revealed accumulation in the spleen and the liver, which was not observed in the control mice (no functionalization; Figure 3A), suggesting bacterial

dissemination. Biodistribution data indicated that these accumulations were significantly ($p < 0.001$) higher for mice with infected livers compared to control mice (27.1 ± 11.1% ID/g vs 7.6 ± 2.3%ID/g) and intestines (19.5 ± 8.7%ID/g vs 2.6 ± 0.5%ID/g) (Figure 3 B, Table S1). Liver−muscle ratios revealed a nearly 6-fold increase for infected mice (20.0 ± 7.8% ID/g vs 3.4 ± 0.8%ID; $p < 0.001$). These data were further corroborated by fluorescence imaging of the liver, showing a higher Cy5 signal in infected (*i*) livers than in uninfected (*ii*) ones (Figure 3C).

To rule out dissociation of the guest-vector ^{99m}Tc-UBI$_{29-41}$-Ad$_2$ from the bacteria, the biodistribution of unbound ^{99m}Tc-UBI$_{29-41}$-Ad$_2$ was separately assessed. Gauged by the ^{99m}Tc signal (Table S3), ^{99m}Tc-UBI$_{29-41}$-Ad$_2$ was cleared via the renal pathway. Thus, as we did not observe ^{99m}Tc-activity in the bladder (Figures 2A, 3A), it appeared that throughout the experiment, ^{99m}Tc-UBI$_{29-41}$-Ad$_2$ remained attached to bacteria. This result was in good agreement with an earlier study of ours.[15]

■ DISCUSSION

In this study, we addressed the feasibility of harnessing cyclodextrin/adamantane (CD/Ad) host−guest chemistry to

achieve targeted accumulation of a chemical cargo. To this end, we functionalized living *S. aureus* bacteria with Ad, inoculated the bacteria into either muscle or liver, and then intravenously administered a chemical cargo to target these Ad-functionalized bacteria. We found that for both muscle and liver models, the presence of Ad-functionalized bacteria (the guest) was able to drive accumulation of the injected chemical cargo (the host). Hence, this study demonstrates a crucial proof-of-principle of the utility offered by supramolecular host–guest chemistry in advancing precision medicine.

While our earlier efforts to translate CD-Ad-based supramolecular host–guest chemistry into *in vivo* applications made use of chemical microspheres designed for hepatic embolization,[10,11] the work presented here uses actual living cells. Furthermore, we show here that the approach has value outside the liver, in this case, being able to target a focal point in the muscle. While the presence of nonfunctionalized bacteria by themselves led to a slight accumulation of the chemical cargo, the accumulation was significantly improved upon by the presence of the Ad functionalization. These results are in line with previous work done in our group, which has shown that bacterial surfaces appear to possess structures capable of serving as a weaker "guest" (analogously to Ad) for binding host-vectors like the CD-polymers used in this study.[14] Despite this property, bacteria nevertheless represented the most intriguing next step to take in developing this technology, because this technology could allow for long-term tracking of bacterial infections in animal models and provide opportunities for exploring targeted treatment modalities which may be grafted onto the CD polymer.

To expand upon this study's findings, future studies will need to further tweak the presented chemical cargo delivery system to increase its clinical value. For instance, while the Ad-functionalization of bacteria in this study took place *in vitro* prior to inoculation into mice to more reliably assess the concept's feasibility, clinical applications will likely depend on an initial *in vivo* Ad-functionalization. To this end, Ad-vectors must be designed to functionalize the target of interest specifically. For targeting bacteria, UBI_{29-41} potentially represents one such vector. In earlier studies, we reported a 10-fold higher binding to bacteria over host cells *in vitro*, which increased to 200-fold *in vivo*.[18] Since then, several other studies have demonstrated that this preferential binding to bacteria is maintained when a range of functionalizations is conjugated to UBI_{29-41}.[16] Other targeting vectors that instead target overexpressed receptors on tumor cells can represent another attractive option for specific *in vivo* Ad-functionalization and would widen the application of the cargo delivery concept beyond infectious diseases.[6] An additional consideration for future clinical applications will be to investigate how compatible the presented chemical cargo delivery system is with various therapeutic agents. Such investigations have recently been initiated in our laboratory, and we hope that the findings presented here will also spur others to investigate supramolecular chemistry as a chemical instrument for advancing precision medicine.

■ CONCLUSION

In conclusion, we have here shown that host–guest chemistry is well-suited for *in vivo* cargo delivery to bacterial inoculations. Further development and refinement of the concept could pave the path toward therapeutic studies and innovative new treatment paradigms.

■ EXPERIMENTAL PROCEDURES

General. All chemicals were obtained from commercial sources and used without further purification. Solvents were obtained from Actu-All Chemicals (Oss, The Netherlands) in HPLC grade and used without further purification. The reactions were monitored by thin-layer chromatography (TLC) and mass spectrometry using a Bruker microflex LRF MALDI-TOF. HPLC was performed on a Waters (Etten-Leur, The Netherlands) HPLC system using a 1525EF pump and a 2489 UV/vis detector. For preparative HPLC, a Dr Maisch GmbH (Ammerbuch, Germany) Reprosil-Pur 120 C18-AQ 10 μm (250 × 20 mm) column was used (12 mL/min). For analytical HPLC, a Dr Maisch GmbH Reprosil-Pur C18-AQ 5 μm (250 × 4.6 mm) column was used, applying a gradient of 0.1% TFA in H_2O/CH_3CN 95:5 to 0.1% TFA in H_2O/ CH_3CN 5:95 in 40 min (1 mL/min).

Synthesis. *UBI_{29-41}-Ad_2.* Synthesis of adamantane-functionalized antimicrobial peptide ubiquicidin, UBI_{29-41}-Ad_2, was carried out as follows (Figure S1). The UBI_{29-41} peptide (H-TGRAKRRMQYNRR-NH_2) was synthesized by Fmoc solid-phase peptide synthesis (SPPS). Four molar equivalents of Fmoc-Lys(Fmoc)–OH, PyBOP, and 1-hydroxybenzotriazole, and 15 mol equiv of DiPEA were dissolved in anhydrous DMF (3 mL), and this mixture was added to the UBI_{29-41} peptide on solid polymer support bearing a free amine on the N-terminal. After 2 h of shaking at room temperature, the solid was washed using DMF, followed by DCM. A bromophenol blue test (BPB) was used to confirm the full conversion. After standard Fmoc deprotection using 20% piperidine in DMF and reswelling of the polymer beads using DCM 4 mol equiv of Fmoc-Gly-OH, PyBOP, 1-hydroxybenzotriazole, and 15 equiv of DiPEA were dissolved in anhydrous DMF (3 mL) and added to the polymer beads. The suspension was shaken at room temperature for 18 h, and then washing, Fmoc deprotection, and reswelling were performed. Again, BPB was used to show full conversion. Hereafter, Fmoc protection and subsequent washing steps were performed, followed by coupling of 1-adamantane-carbonyl chloride (4 equiv) using DiPEA (15 equiv) and HOBt (4 equiv). Following confirmation by BPB and washing steps, the final product and protective groups were cleaved using TFA/TIPS/H_2O 38:1:1 and purified by preparative HPLC. After pooling the relevant fractions and lyophilization, a white solid was obtained; MALDI-TOF $[M + H]^+$ calculated: 2258.7; found 2285.2. An analytical HPLC chromatogram is shown in Figure S2.

$Cy5_{0.5}CD_9PIBMA_{39}$. Synthesis and characterization of Cy5 functionalized β-cyclodextrin-poly(isobutylene-*alt*-maleic-anhydride) ($Cy5_{0.5}CD_9PIBMA_{39}$, ~18.7 kDa, diameter ~11.7 nm) was carried out as previously described.[6]

Radiolabeling and Stability Testing. *Radiolabeling of Guest Vector UBI_{29-41}-Ad_2 with ^{99m}Tc.* Radiolabeling of UBI_{29-41}-Ad_2 with ^{99m}Tc (^{99m}Tc-UBI_{29-41}-Ad_2) and stability of the ^{99m}Tc-chelation were carried out as follows: to 5 μL of UBI_{29-41}-Cy5-Ad_2 (797 μM/mL H_2O), 4 μL of $SnCl_2$·$2H_2O$ (0.44 mg/mL saline, Technescan PYP, Mallinckrodt Medical B.V. Petten, The Netherlands), 4 μL of NaOH (0.1 M), and 100 μL of a freshly eluted ^{99m}Tc–Na-pertechnetate solution (1000 MBq/mL, Mallinckrodt Medical B.V.) were added, and the mixture was gently stirred in a shaking water bath for 1 h at 37 °C.[15,18] The schematic structure of ^{99m}Tc-UBI_{29-41}-Ad_2 is depicted in Figure S3. The stability of the radiolabeling was

determined at 37 °C at various intervals up to 24 h in 1 mL of PBS or fetal calf serum (20% vol/vol, FCS, Life Technologies Inc. CA). The release of radioactivity was assessed by instant thin-layer chromatography (ITLC) on 1 × 7 cm ITLC-SG paper strips (Agilent Technologies, USA) using PBS as the mobile phase (Figure S4A).

Radiolabeling of $Cy5_{0.5}CD_9PIBMA_{39}$ with ^{111}In. Labeling of $Cy5_{0.5}CD_9PIBMA_{39}$ and stability testing of host-vector ^{111}In-$Cy5_{0.5}CD_9PIBMA_{39}$ was carried out as previously described.[10,11]

Labeling of S. aureus with ^{99m}Tc-UBI_{29-41}-Ad_2. To allow imaging of the administered bacteria in a whole mouse model, *S. aureus* (ATCC 25922) was labeled with the primary guest-vector ^{99m}Tc-UBI_{29-41}-Ad_2 as was previously used for labeling with the hybrid tracer ^{99m}Tc-UBI_{29-41}-Cy5 [15]. In short, 100 μL of ^{99m}Tc-UBI_{29-41}-Ad_2 (20−100 MBq) was added to 1 mL of *S. aureus* (1×10^8 CFU/mL in 25 mM Na-NH$_4$-acetate buffer pH 5), and the mixture was gently stirred at room temperature. The efficiency of the rate of bacterial functionalization was measured at different intervals within a 24 h time frame. Before determining the tracer uptake at each interval, 0.1 mL of the bacteria in the labeling suspension was washed two times with phosphate-buffered saline (PBS) and centrifugation steps (4 min × 3500 rpm). The amount of radioactivity associated with bacteria was determined at various intervals. The efficiency of the bacterial functionalization was expressed as the % of the total added amount of radioactivity: $((([MBq]_{added}/[MBq]_{associated\ with\ bacteria}) \times 100)$.[15]

In Vitro Host−Guest Interactions. Mixtures of 0.1 mL containing 37 nmol UBI_{29-41}-Ad_2 labeled to 1×10^8 colony forming units (CFU) of *S. aureus* were incubated with 0.1 mL ^{111}In-$Cy5_{0.5}CD_9PIBMA_{39}$ (10 μg/mL, 1 MBq) and 0.8 mL of PBS. The mixtures were incubated for 1 h in a shaking water bath at 37 °C. Cells were washed after spinning twice for 5 min at 1500 × g and resuspending the pellet with PBS. The decay-corrected radioactivity associated with the pellet containing the bacteria and the supernatant was measured in a dose calibrator (VDC101, Veenstra Instruments, Joure, The Netherlands). Following correction for background activity, the host−guest interaction was expressed as the percentage of the total amount of radioactivity binding to the bacterial pellet. As a specificity control, nonspecific binding of ^{111}In-$Cy5_{0.5}CD_9PIBMA_{39}$ to the same number of bacteria without UBI_{29-41}-Ad_2 labeling was evaluated.

Confocal Microscopy. Confocal microscopy was used to confirm the *in vitro* accumulation of $Cy5_{0.5}CD_9PIBMA_{39}$ on UBI_{29-41}-Ad_2 labeled bacteria. 0.2 mL of 25 mM Na-NH$_4$-acetate buffer pH 5 solution containing 1×10^8 CFUs *S. aureus*, 10 μM UBI_{29-41}-Ad_2, and 10 μM Hoechst 33342 was incubated for 30 min in a dark shaking water bath at 37 °C. Samples were washed twice in PBS as described above, after which they were incubated in 0.2 mL of a 1 μM solution of $Cy5_{0.5}CD_9PIBMA_{39}$ for 60 min in a dark shaking water bath at 37 °C. Samples were washed thrice in PBS as described above, and finally resuspended in 100 μL PBS. Ten microliters of labeled bacteria were pipetted onto culture dishes with glass inserts (ø35 mm glass-bottom dishes No. 15, poly(D-lysine) coated, γ-irradiated, MatTek Corporation). Images were acquired at intervals of 1, 4, and 24 h in a single field of view using a Leica SP8 WLL confocal microscope (λex 633 nm, λem 650−700 nm) under 100× magnification using Leica Application Suite Software Suite 4.8. Pictures were loaded in ImageJ software (ImageJ 1.44p, NIH, USA) to draw a profile

line over a single representative stained bacterium in the Cy5 and the Hoechst spectrum to estimate the distribution of both dyes in the bacterial membrane and cytoplasm.

In Vivo Imaging Experiments. Animals. In vivo studies were performed using 2−4-month-old Swiss mice (20−35 g, Crl:OF1 strain, Charles River Laboratories, USA). All animal studies were approved by the Institutional Animal Ethics Committee (DEC permit 12160) of the Leiden University Medical Center (LUMC). Mice were kept under specific pathogen-free conditions in the animal housing facility of the LUMC. Food and water were provided *ad libitum*. Two models were used: a thigh muscle and a hepatic embolization model.

For Muscle Inoculation. Mice were injected in the right thigh muscle with 0.1 mL of ^{99m}Tc-UBI_{29-41}-Ad_2-labeled *S. aureus* (n = 6). After 24 h, 0.1 mL secondary vector (host), ^{111}In-$Cy5_{0.5}CD_9PIBMA_{39}$ (10 μg/mL, approximately 15 MBq), was i.v. administered. As controls for the muscle model, 6 mice were either infected with nonfunctionalized *S. aureus* to demonstrate nonspecific uptake of the secondary vector or not infected at all, to study the general biodistribution of ^{111}In-$Cy5_{0.5}CD_9PIBMA_{39}$.

For Liver Inoculation. A liver embolization setup was performed according to previously described procedures.[10,11] In brief, animals were anaesthetized by intraperitoneal injection of a mixture containing Hypnorm (Vetapharma, Leeds, United Kingdom), dormicum (Roche, Basel, Switzerland), and water (1:1:2). After shaving and cleaning with ethanol (70%), the abdominal cavity was incised for 0.5 cm, and the spleen was exposed outside the peritoneum. After that, 1×10^8 CFU ^{99m}Tc-UBI_{29-41}-Ad_2-labeled *S. aureus* in a volume of 0.1 mL (5 MBq) was slowly injected into the spleen of mice (n = 6) using a Myjector U-100 insulin syringe (29G × 1/2 in. 0.33 × 12 mm, Terumo Europe, Leuven, Belgium). After 5 s, the needle was removed, and the spleen was repositioned in the peritoneal cavity. 2−4 stitches sutured the incision, and the animals were placed under a heating lamp to maintain until recovery. After 24 h, 0.1 mL ^{111}In-$Cy5_{0.5}CD_9PIBMA_{39}$ (10 μg/mL, approximately 15 MBq) was administered intravenously (i.v.). Here, mice with noninfected livers were included as a control study (n = 6) as we studied the nonspecific uptake to bacteria *in vivo* and the general biodistribution of ^{111}In-$Cy5_{0.5}CD_9PIBMA_{39}$ already in the muscle inoculation model.

Imaging Studies and Biodistribution Assays. SPECT imaging of mice either intramuscularly or hepatically inoculated by ^{99m}Tc-UBI_{29-41}-Ad_2-labeled *S. aureus* was performed[15,19] using a U-SPECT-2 scanner and continuous 1−2% isoflurane anesthesia, with imaging of ^{111}In-$Cy5_{0.5}CD_9PIBMA_{39}$ in mice with non-UBI_{29-41} functionalized *S. aureus* and without bacterial infection as a control. Image acquisition took 20 min, and images were reconstructed according to the optimized settings for ^{99m}Tc (140 keV) and ^{111}In (170 and 240 keV). Mice were imaged 4 h after the administration of ^{111}In-$Cy5_{0.5}CD_9PIBMA_{39}$ using SPECT. After imaging, mice were euthanized by an intraperitoneal injection of 0.25 mL Euthasol (ASTfarma, Oudewater, The Netherlands). Tissues were excised for use in quantitative biodistribution studies. Various organs and tissues were weighed and counted for their radioactive content using a gamma counter (2470 automatic gamma counter, Perkin−Elmer). Counts per minute were converted into decay-corrected MBq at the time point of injection (t = 0), and the percentage of the injected dose per gram of tissue (%ID/g) was calculated as follows: $((([MBq]_{tissue}/[MBq]_{injected}) \times$

100)/g tissue). From biodistribution data, infection-to-background ratios and the % of excreted radioactivity were determined. To calculate the amount of excreted radioactivity, the entire mouse was weighed and counted for radioactivity in a dose-calibrator. At the time of dissection, and after the removal of various tissues, the radioactivity in the mouse was recalculated. Excreted radioactivity (in urine and feces) was then calculated as (radioactivity of injected dose) − (radioactivity of excised tissues + radioactivity carcass). To determine the biodistribution of free ^{99m}Tc-UBI$_{29-41}$-Ad$_2$ (not associated with *S. aureus*), three noninfected mice were injected and imaged as described above.

Ex vivo fluorescence imaging of excised infected and noninfected tissues of both models was carried out using the IVIS Spectrum imaging system (Caliper Life Science, Hopkinton, MA).[19] This helped verify the localization of the hybrid polymer via optical imaging.

Statistical Analysis. All data are presented as mean value (±SD) of 3−6 independent measurements. Student's two-tailed independent sample t test was used to performed statistical analysis for differences between groups in the animal studies. Significance was assigned for p-values <0.05. All analyses and calculations were performed using Microsoft Office Excel 2010 and GraphPad Prism ver. 5.01 for Windows (GraphPad Software, San Diego, CA, USA).

■ ASSOCIATED CONTENT

Ⓢ Supporting Information

The Supporting Information is available free of charge at https://pubs.acs.org/doi/10.1021/acs.bioconjchem.1c00061.

Chemical synthesis pathway, schematic depiction, and radiolabeling; HPLC; Biodistribution of radiolabeled vectors (tables) (PDF)

■ AUTHOR INFORMATION

Corresponding Author

Fijs W. B. van Leeuwen − *Interventional Molecular Imaging Laboratory, Department of Radiology, Leiden University Medical Center, 2300 RC Leiden, Netherlands;* ⓞ orcid.org/0000-0002-6844-4025; Email: f.w.b.van_leeuwen@lumc.nl

Authors

Mick M. Welling − *Interventional Molecular Imaging Laboratory, Department of Radiology, Leiden University Medical Center, 2300 RC Leiden, Netherlands;* ⓞ orcid.org/0000-0002-2249-5601

Nikolas Duszenko − *Interventional Molecular Imaging Laboratory, Department of Radiology and Department of Parasitology and Infectious Diseases, Leiden University Medical Center, 2300 RC Leiden, Netherlands;* ⓞ orcid.org/0000-0001-7860-1242

Danny M. van Willigen − *Interventional Molecular Imaging Laboratory, Department of Radiology, Leiden University Medical Center, 2300 RC Leiden, Netherlands*

Wiep Klaas Smits − *Department of Medical Microbiology, Section Experimental Bacteriology, Leiden University Medical Center, 2300 RC Leiden, Netherlands;* ⓞ orcid.org/0000-0002-7409-2847

Tessa Buckle − *Interventional Molecular Imaging Laboratory, Department of Radiology, Leiden University Medical Center,*

2300 RC Leiden, Netherlands; ⓞ orcid.org/0000-0003-2980-6895

Meta Roestenberg − *Department of Parasitology and Infectious Diseases, Leiden University Medical Center, 2300 RC Leiden, Netherlands*

Complete contact information is available at:
https://pubs.acs.org/10.1021/acs.bioconjchem.1c00061

Notes

The authors declare no competing financial interest.

■ ACKNOWLEDGMENTS

■ REFERENCES

(1) Yu, G., and Chen, X. (2019) Host-guest chemistry in supramolecular theranostics. *Theranostics* 9, 3041−3047.

(2) Lai, W.-F., Rogach, A. L., and Wong, W.-T. (2017) Chemistry and engineering of cyclodextrins for molecular imaging. *Chem. Soc. Rev.* 46, 6379−6419.

(3) Saokham, P., Muankaew, C., Jansook, P., and Loftsson, T. (2018) Solubility of cyclodextrins and drug/cyclodextrin complexes. *Molecules* 23, 1161.

(4) Paolino, M., Ennen, F., Lamponi, S., Cernescu, M., Voit, B., Cappelli, A., Appelhans, D., and Komber, H. (2013) Cyclodextrin-adamantane host-guest interactions on the surface of biocompatible adamantyl-modified glycodendrimers. *Macromolecules* 46, 3215−3227.

(5) Challa, R., Ahuja, A., Ali, J., and Khar, R. K. (2005) Cyclodextrins in drug delivery: An updated review. *AAPS PharmSciTech* 6, E329−E357.

(6) Rood, M. T. M., Spa, S. J., Welling, M. M., ten Hove, J. B., van Willigen, D. M., Buckle, T., Velders, A. H., and van Leeuwen, F. W. B. (2017) Obtaining control of cell surface functionalizations via pre-targeting and supramolecular host-guest interactions. *Sci. Rep.* 7, 39908.

(7) Wu, Z., Song, N., Menz, R., Pingali, B., Yang, Y. W., and Zheng, Y. (2015) Nanoparticles functionalized with supramolecular host-guest systems for nanomedicine and healthcare. *Nanomedicine (London, U. K.)* 10, 1493−514.

(8) Li, Q., Wu, Y., Lu, H., Wu, X., Chen, S., Song, N., Yang, Y.-W., and Gao, H. (2017) Construction of supramolecular nanoassembly for responsive bacterial elimination and effective bacterial detection. *ACS Appl. Mater. Interfaces* 9, 10180−10189.

(9) Sankaran, S., van Weerd, J., Voskuhl, J., Karperien, M., and Jonkheijm, P. (2015) Photoresponsive cucurbit[8]uril-mediated adhesion of bacteria on supported lipid bilayers. *Small* 11, 6187−96.

(10) Spa, S. J., Welling, M. M., van Oosterom, M. N., Rietbergen, D. D. D., Burgmans, M. C., Verboom, W., Huskens, J., Buckle, T., and van Leeuwen, F. W. B. (2018) A supramolecular approach for liver radioembolization. *Theranostics* 8, 2377−2386.

(11) Welling, M. M., Spa, S. J., van Willigen, D. M., Rietbergen, D. D. D., Roestenberg, M., Buckle, T., and van Leeuwen, F. W. B. (2019) In vivo stability of supramolecular host-guest complexes monitored by dual-isotope multiplexing in a pre-targeting model of experimental liver radioembolization. *J. Control. Release* 293, 126−134.

(12) Welling, M. M., Duszenko, N., van Willigen, D. M., Hensbergen, A. W., Buckle, T., Rietbergen, D. D. D., Roestenberg, M., and van Leeuwen, F. W. B. (2021) (Accepted) Interventional Nuclear Medicine: "click" chemistry as an in vivo pre-targeting strategy for imaging microspheres and bacteria. *Biomater. Sci.*, 1 DOI: 10.1039/D0BM01823F.

(13) Strebl, M. G., Yang, J., Isaacs, L., and Hooker, J. M. (2018) Adamantane/Cucurbituril: A potential pretargeted imaging strategy in immuno-PET. *Mol. Imaging 17*, 153601211879983.

(14) Duszenko, N., van Willigen, D. M., Welling, M. M., de Korne, C. M., van Schuijlenburg, R., Winkel, B. M. F., van Leeuwen, F. W. B., and Roestenberg, M. (2020) A supramolecular platform technology for bacterial cell surface modification. *ACS Infect. Dis. 6*, 1734−1744.

(15) Welling, M. M., de Korne, C. M., Spa, S. J., van Willigen, D. M., Hensbergen, A. W., Bunschoten, A., Duszenko, N., Smits, W. K., Roestenberg, M., and van Leeuwen, F. W. B. (2019) Multimodal tracking of controlled Staphylococcus aureus infections in mice. *ACS Infect. Dis. 5*, 1160−1168.

(16) Welling, M. M., Hensbergen, A. W., Bunschoten, A., Velders, A. H., Roestenberg, M., and van Leeuwen, F. W. B. (2019) An update on radiotracer development for molecular imaging of bacterial infections. *Clin. Transl. Imaging 7*, 105−124.

(17) Welling, M. M., Hensbergen, A. W., Bunschoten, A., Velders, A. H., Scheper, H., Smits, W. K., Roestenberg, M., and van Leeuwen, F. W. B. (2019) Fluorescent imaging of bacterial infections and recent advances made with multimodal radiopharmaceuticals. *Clin. Transl. Imaging 7*, 125−138.

(18) Welling, M. M., Paulusma-Annema, A., Balter, H. S., Pauwels, E. K. J., and Nibbering, P. H. (2000) Technetium-99m labelled antimicrobial peptides discriminate between bacterial infections and sterile inflammations. *Eur. J. Nucl. Med. Mol. Imaging 27*, 292−301.

(19) Welling, M. M., Bunschoten, A., Kuil, J., Nelissen, R., Beekman, F. J., Buckle, T., and van Leeuwen, F. W. B. (2015) Development of a hybrid tracer for SPECT and optical imaging of bacterial infections. *Bioconjugate Chem. 26*, 839−849.